



JOURNAL OF BIOMEDICAL ENGINEERING AND MEDICAL IMAGING

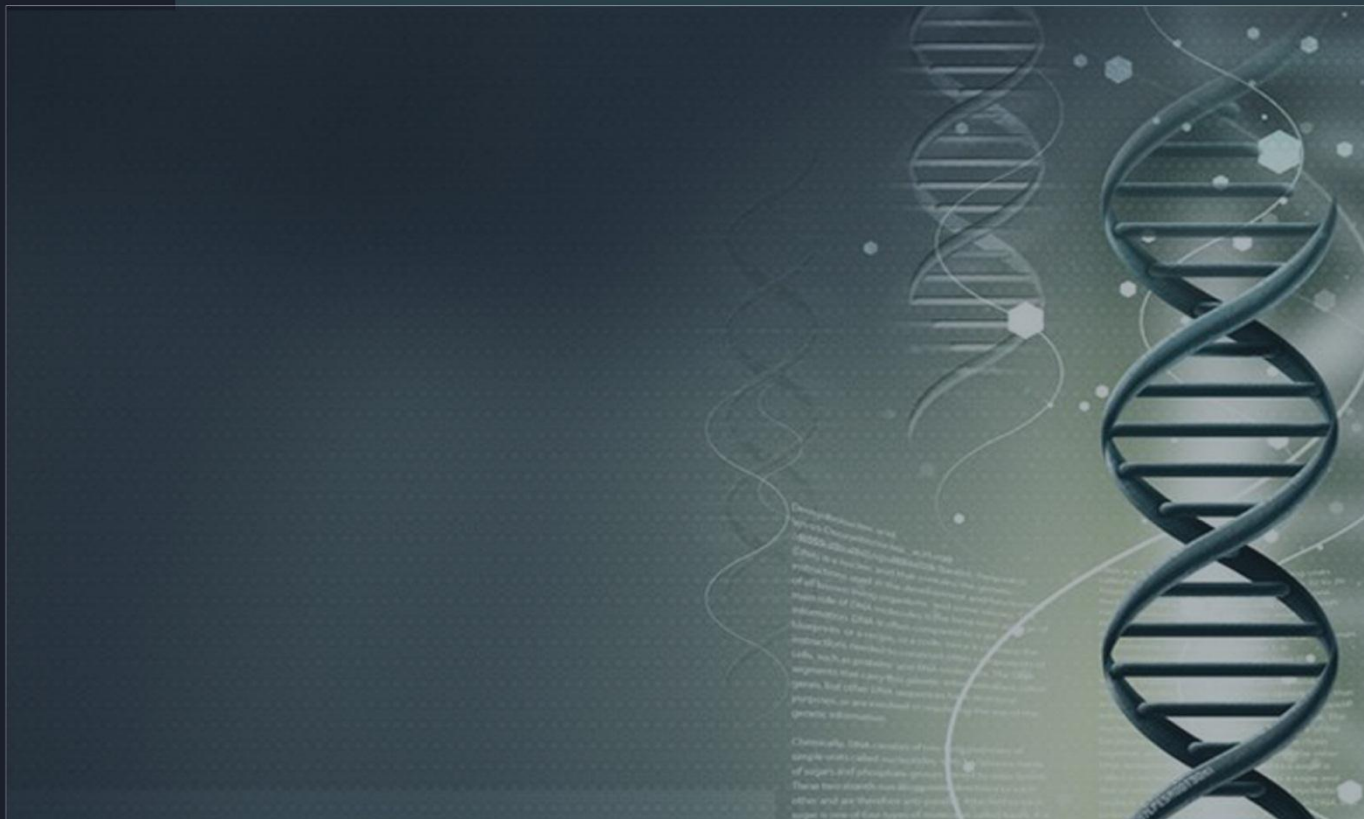


TABLE OF CONTENTS

EDITORIAL ADVISORY BOARD	I
DISCLAIMER	II
Novel Approach for Noise Removal of Brain Tumor MRI Images	
D. Anithadevi	1
K. Perumal	
An Accurate Liver Segmentation Method Using Parallel Computing Algorithm	15
Yousif Mohamed Y. Abdallah	
A Comparative Study of Shear-Wave Elastography and Strain Elastography on a Breast Phantom for Diagnosis of Tumor and Cyst	
Mahdi Al-Qahtani,	24
Eraj Humayun Mirza,	
Mubarak Dhafer Al-Qahtani	
Mohammed Fahad Al-Muqati	
Designing of Computer Aided Diagnostic System for the Identification of Exudates in Retinal Fundus Images	
Santosh Kumar Mishra,	29
Deepthi Mittal and Ramesh Kumar Sunkaria	

EDITORIAL ADVISORY BOARD

Professor Kenji Suzuki

Department of Radiology, University of Chicago
United States

Professor Habib Zaidi

Dept. of Radiology, Div. of Nuclear Medicine, Geneva University Hospital, Geneva, Swaziland

Professor Tzung-Pe

National University of Kaohsiung,, Taiwan
China

Professor Nicoladie Tam

Dept. of Biological Sciences, University of North Texas, Denton, Texas, United States

Professor David J Yang

The University of Texas MD Anderson Cancer Center, Houston
United States

Professor Ge Wang

Biomedical Imaging Center, Rensselaer Polytechnic Institute. Troy, New York
United States

Dr Hafiz M. R. Khan

Department of Biostatistics, Florida International University
United States

Dr Saad Zakko

Director of Nuclear Medicine Dubai Hospital
UAE

Dr Abdul Basit

Malaysia School of Information Technology, Monash University
Malaysia

DISCLAIMER

All the contributions are published in good faith and intentions to promote and encourage research activities around the globe. The contributions are property of their respective authors/owners and the journal is not responsible for any content that hurts someone's views or feelings etc.

Novel Approach for Noise Removal of Brain Tumor MRI Images

D. Anithadevi and K. Perumal

Department of Computer Applications, Madurai Kamaraj University,
danithatce@gmail.com

ABSTRACT

In Image processing, Image denoising becomes mandatory for many applications. In medical imaging, An MRI (Magnetic Resonance Imaging) image provides high quality when estimated with CT imaging techniques and hence it is best suited for diagnosis. Even though it's providing high quality informations, images may corrupted by noise due to acquisition and transmission. Noises have to remove while the mean time there is no loss of information and also have the capability to preserve edges. This paper presents a novel approach for denoise the brain tumor MRI images using combine features of Stationary Wavelet Transform (SWT), median filter and sharpening filter. Accordingly, this approach is intended to develop for the noise removal with the edge preserving qualities in brain tumor MRI images. In Wavelet, SWT shows a superior performance in denoising because of its multi-resolution property and no signal leakage. Median filter helps in preserving edges and edges are enhanced by sharpen filter .And the results are compared using some image quality factors to find out the similarity with the original images.

Key words —Wavelet transform, Image denoising, Sharpen filter, Median filter.

1 Introduction

Image denoising is the most significant steps to remove the noise in an image that leads to provide good results in an image processing. Normally MRI images provide high quality when compared to CT (Computed Tomography) imaging techniques. So it is best suited for medical diagnosis. Even if an MRI image provides high quality that is also corrupted with some noises such as impulse noise, speckle noise, blur noise (unexpectedly patients shaking their heads during scanning the brain) during acquisition and transmission [14]. So denoising technique is needs to remove the noise from the image, which is applicable for further processing such as segmentation, classification, etc. Moreover edges are important features for MRI images. The most important in image denoising is to preserve the edges and all fine details of an image during noise reduction [10].

Median filtering is used to remove salt and pepper noise because of its effective noise suppression capability and computational efficiency. This filter tends to preserve edges during filtering. However, this median filter is performed poorly in the presence of signal dependent noise [9]. Wavelet transform is a tool for denoising the image. It endeavors to remove the noise present in the signal while preserving the characteristics of signal of its frequency content. This work contains various wavelet types with median filtered image and that are used for sharpen filter to enhance the edge features of an image [12].

Wavelets being used more and more because that are capable of deconstructing complex signals into basis signals of bandwidth and then reconstructing it again with very little loss of information [1]. Particularly this means there is little to no signal leakage of phase-shifting of the original signal when decompose it. Conventional filters generally have problems with signal leakage of phase-shifting that have to be dealt with least acknowledge in the output. The SWT is designed to overcome the drawbacks of DWT. So this SWT is used for denoising the brain images. The main objective is to remove noise in MRI images without loss of any information and preserve edge features.

2 Literature Review

Kanwaljeet Kaur et.al [5], worked with the spatial filter like median [8] and weiner filter, etc. and disadvantage of median filter is the extra computation time needed to sort the intensity value of each set. Rong Zhu et al [9] has discussed about various median filtering techniques and which filters works well with the noise and which filter having edge preserving quality while removing noise and they proposed improved median filtering techniques that works well than other filters. It smoothen the edge information to overcome this drawback Abdulla Al Juma [1] worked with wavelet transform is used to remove the noise information in the signal without loss of image originality [6]. Jaspreet kaur et al [4] proposed a novel approach to denoising the speckle noise in ultrasound images using DWT and that is used for FCM based segmentation. Here the drawback is time invariant and loss of information due to down sampling to overcome these drawback S.Janani et al [3] worked with the SWT filter. There is no sub sampling so no loss of its originality. They processed a new approach for segmentation based on SWT and FCM. Mirajkar PradnyaP, et al [6], V N Prudhvi Raj, et al [7] worked with wavelet transform for denoising and image fusion. Rupinderpal Kaur, et al[10] worked with denoising the medical images using DWT. Soundarya K [13] worked with the SWT based noise removal using video processing images. A. Velayudham et al [14] has been worked with medical image denoising [15]. Types of noises corrupted the medical images which denoising techniques are provided good denoised images that are researched by them. Quality assessment of spatial filtering techniques has been discussed [11] and various types of quality metrics used to measures the dissimilarity between the input images and denoised images are also discussed in [2] and region based segmentation is used to extract the brain tumor images along with the morphological operator.

3 Proposed Work

The main intention of the work is to reduce noises in the MRI images without loss of information. So, for this work we proposed a novel approach that is combined features of three filters such as median filter, SWT and Unsharp masking filter. Basically MRI images may corrupt salt and pepper noise during acquisition and transmission. Median filter is well performed with all types of impulse noise. Wavelets help denoising the image without loss of its originality. So Wavelet based denoising technique is applied in the gray image. Although these filters are removing noises and also preserve edges of an image that also need to enhance the edges so, sharpen filter is used. The result of novel approach denoised image is used to measure the quality using various quality metrics with its original image. During quality measurements dissimilarity of the pixels of denoised image is identified. And the novel approach is compared with the existing filters of median filter and the combinations of median and SWT filters and how the novel approach result is better than other filters results that discussed.

4 Methodology

In this novel approach three types of filtering techniques are used to remove noises while the mean time enhances the edges of an image. The denoised image has got from original image subtracted with noise. So it can preserve edge features. Combine features of the filters such as

- Median Filter
- SWT Filter
- Unsharp Filter

4.1 Denoising Procedure:

The procedure to denoise an image is given as follows:

- Step1: Convert input image into grayscale image with standard window size.
- Step2: Apply Median Filter to the MRI brain image.
- Step3: Apply stationary wavelet transform with the image.
- Step4: Decompose the image to remove noise.
- Step5: Apply inverse Stationary Wavelet Transform to get a denoised image.
- Step6: Combine the result of median and SWT filters
- Step7: Apply Unsharp masking filter with the combined denoised image.

$$\text{Denoised Image } g(x,y) = \text{Original Image } f(x,y) - \text{noise } n(x,y)$$

Obtain a sharp image by subtracting a lowpass filtered(i.e., smoothed) image from the denoised image:

$$\text{Enhanced denoised image} = \text{DenoisedImage} - \text{smoothed information}$$

Over all block diagram of the work is shown in figure 1

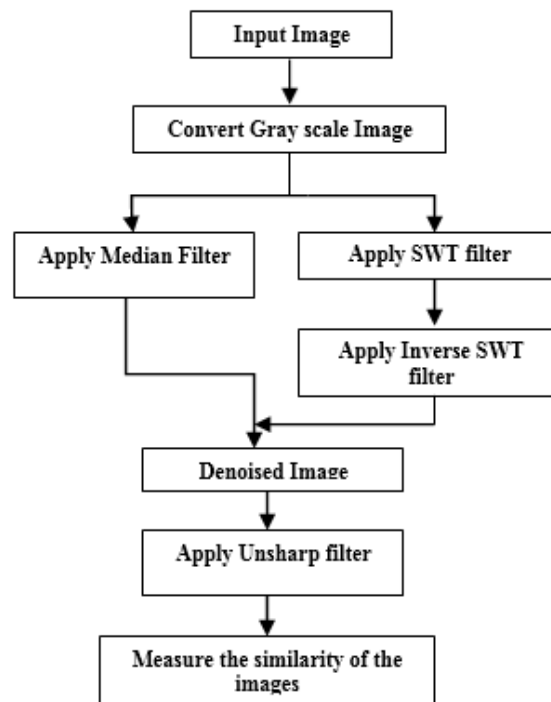


Figure 1: Block diagram of the denoising using combinations of filters.

5 Novel Approach Filtering Techniques

5.1 Median Filter

MRI image may corrupted by salt and pepper noise and random valued noises. Noises may arise due to the changes of transmission of an image. Median filtering is a nonlinear process useful in reducing impulsive or salt-and-pepper noise. It is also useful in preserving edges in an image while reducing random noise [2, 5]. Impulsive or salt-and pepper noise can occur due to a random bit error in a communication channel. In a median filter, a window slides along the image, and the median intensity value of the pixels within the window becomes the output intensity of the pixel being processed.

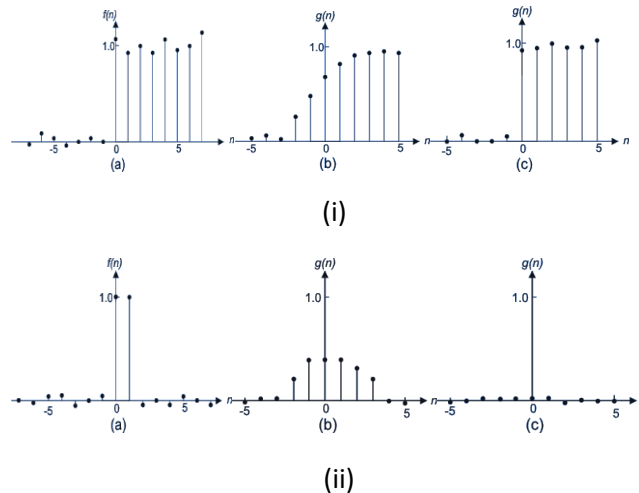


Figure 2: (i,ii) Filtering the 1D signal with 5 point median filter

Like lowpass filtering, median filtering smooths the image and is thus useful in reducing noise. Unlike lowpass filtering, median filtering can preserve discontinuities in a step function and can smooth a few pixels whose values differ significantly from their surroundings without affecting the other pixels. Figure (2(i)a) shows a 1-D step sequence degraded by a small amount of random noise. Figure (2(i)b) shows the result after filtering with a lowpass filter whose impulse response is a 5-point rectangular window. Figure (2(i)c) shows the result after filtering with 5-point median filter. It is clear from the figure that the step discontinuity is better preserved by the median filter. Figure (2ia) shows a 1-D sequence with two values that are significantly different from the surrounding points. Figures (b) and (c) show the result of a lowpass filter and a median filter, respectively. The filters used in figure (2(ii)) are the same as those used in figure (2(i)). If the two impulsive values are due to noise, the result of using a median filter will be reducing the noise. If the two values are part of the signal, however, using the median filter will distort the signal. To prevail over this problem go for wavelet transform.

5.2 Wavelet Transform

Wavelet transform is a tool to represents the image in multiple resolutions. Wavelet transform is used for denoising the signal frequency. So loss of information is avoided. The computation of an image requires filtering and sub-sampling. In each level of sub sampling there are three detail images such as horizontal, vertical, and diagonal informations in high frequency [1]. The decomposition allows a perfect

reconstruction of the original image. There are various types of wavelet transforms among them SWT is the improved version of DWT.

In DWT there is up and down sampling to denoising the image, so information may loss due to down sampling. The stationary wavelet transform is designed to overcome the disadvantages of discrete wavelet transform such as sub sampling the image, there is no translation invariant. There is no down sampling take place between levels. This provides better time frequency localization. DWT and SWT process designed diagram is shown in figure 2.

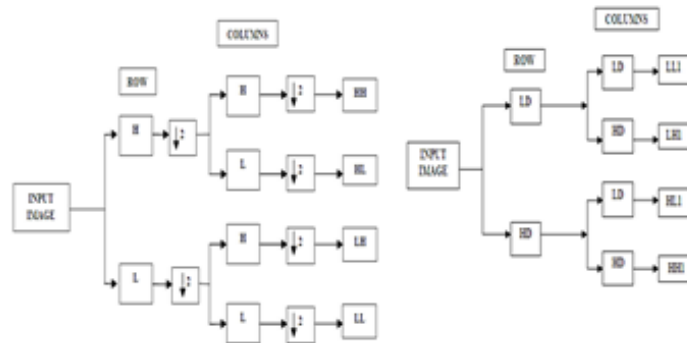


Figure 3: Filter bank structure of the DWT & SWT.

Wavelet decomposition preserved and depicted the sharp transition in images, which results in very accurate denoising in images. So there is no loss of information. These properties of the stationary wavelet transform make the image effective for denoising. Now-a-days multi resolution wavelet denoising techniques are used such as haar, daubechies, Symlet, coiflets, orthogonal and bi-orthogonal [4]. Wavelet thresholding approach is sensitive to denoising. There is two thresholding hard and soft. In hard thresholding, All co-efficient whose magnitude is greater than the selected threshold value that remains same and the other whose magnitude is smaller than the threshold value are set to zero. In soft thresholding all co-efficient who magnitude is greater than the selected threshold value are shrunk towards zero by an amount of threshold and others set to zero. Inverse transform is used to reconstruct the denoised image after decomposition of the original image. The result of median and SWT filters are combined for edge enhancements. The SWT filters process flow diagram is mentioned in figure3.

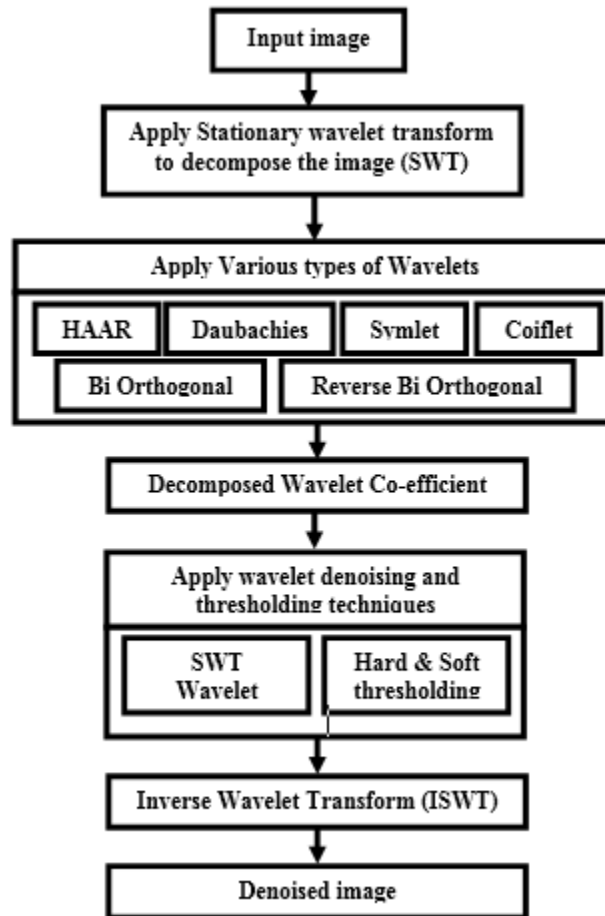


Figure 4: Process flow diagram for SWT denoised Image.

5.2.1 Unsharp Masking

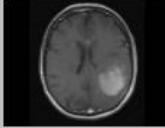
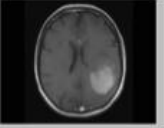
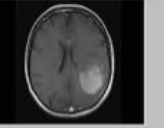
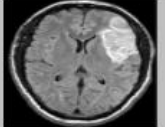
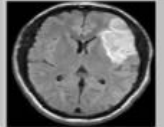
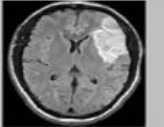
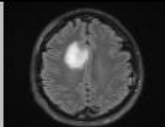
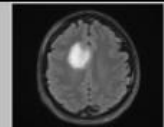
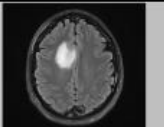
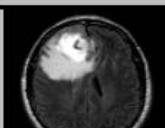
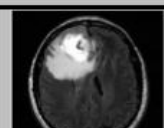
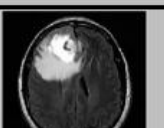
Digital unsharp masking is a flexible and powerful way to increase the sharpness, especially in scanned images. Unfortunately it may create unwanted conspicuous edge effects, or increase image noise. However, these effects can be used creatively, especially if a single channel of an image is sharpened. Undesired effects can be reduced by using a mask [12].

6 Experimental Results and Analysis

6.1 Experimental Results

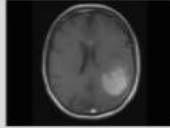
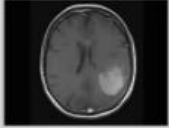
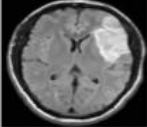
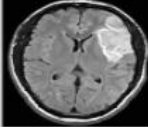
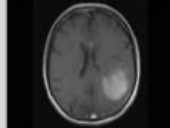
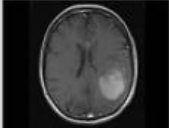
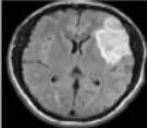
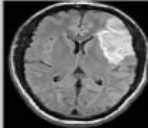
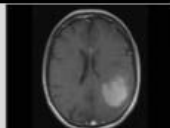
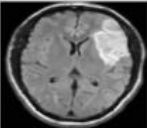
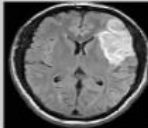
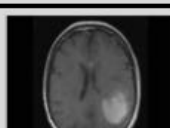
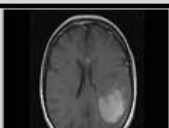
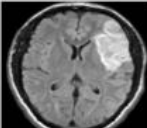
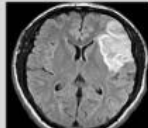
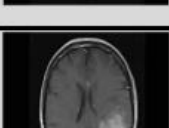
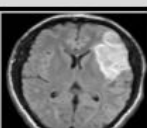
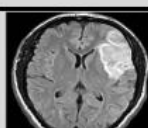
MRI brain tumor images are taken as an input image. In the 2nd column of denoised images are combine features of Median and SWT filters. Images which are in the En.denoised images are the results of novel method. These results are shown in table 1. From this result haar transform works better with this novel approach. The statistical measurement is shown in table 3.

Table 1: Denoised images of various MRI brain Images using Haar wavelet transform.

Input Image	Denoised Image	En.denoised Image
Image1		
		
Image2		
		
Image3		
		
Image4		
		
Image5		

In table 2, MRI brain tumor images are compared with various types of wavelet techniques. Image1 and Image2 are taken as an input image from table 1. Column 2-denoised images are the result of combined features of median and SWT filters. Column 3-En.denoised images are the result of edge enhanced denoised images with various wavelet techniques. Among this which wavelet transform is working well with novel approach that statistical report is given in table 4 and 5.

Table 2: a, b are Various wavelet techniques used for denoising the different MRI images.

Wavelet types	Image1		Wavelet types	Image2	
Daubachies Transform			Daubachies Transform		
Symlet Transform			Symlet Transform		
Coiflet Transform			Coiflet Transform		
Biorthogonal Transform			Biorthogonal Transform		
Reverse Biorthogonal Transform			Reverse Biorthogonal Transform		

(a)

(b)

6.2 Image Quality Parameters for Analysis

Image Quality Measurement (IQM) is essential in the development of image processing algorithms such as deblurring, denoising etc. as it can be used to estimate their performances in terms of quality of processed image. In image processing, the image quality parameters are applied for the evaluation of the imaging system. In fact, in image enhancement system, the truly characteristic measure of image quality is perceptual quality.

The quality of the output image can be tested by exploiting the differences between the corresponding pixels in the test and the output images. Average Difference (AD), Maximum Difference (MD), Normalized Absolute Error (NAE), Signal-to-Noise Ratio (SNR), Mean Square Error (MSE), Mean Absolute Error (MAE), Peak Mean Square Error (PSNR), Structural Content (SC) and Normalized Cross Correlation (NCC) are examples IQM measures. These measures measure the dissimilarity between the two images on the basis of comparing the corresponding pixels of the two images.

6.2.1 Mean Squared Error (MSE)

Mean Squared Error (MSE) is the average squared difference between input and denoised output image. The error is the amount by which the value obscure by the estimator differs from the quantity to be

estimated. The image quality parameters used in this work for comparing the denoised result with the original image. It is expressed as

$$MSE = \frac{1}{MN} \sum_{j=1}^M \sum_{k=1}^N (x_{j,k} - x'_{j,k})^2$$

Where x is the original image and x' is the denoised image, Where M and N is number of rows and columns of the image. The quality of the tested image should have MSE values lower as the lowest error rate, so that it is having good result [12].

6.2.2 Peak Signal-To-Noise Ratio (PSNR)

Peak signal-to-noise ratio (PSNR) is the ratio between the maximum possible power of a signal and the power of corrupting noise that affects the reliability of its representation. PSNR is the evaluation standard of the reconstructed image quality. The PSNR represents a measure of the peak value of the error. If MSE is zero, then PSNR is infinity. This means that a high value of the PSNR provides a higher image quality [12]. Similarly, the smaller value of the PSNR implies that the difference between the images is larger and the image quality is lower. It is expressed as

$$PSNR = 10 \log \frac{(2^n - 1)^2}{MSE} = 10 \log \frac{255^2}{MSE}$$

Where 255 is maximum possible value that can be attained by the image signal and MSE is mean square error, using this only PSNR will be calculated.

6.2.3 Normalized Cross Correlation (NK/NCC)

Normalized Cross Correlation is a measure of similarity of two images as a function of a time-lag applied to any one of them. It is co relational based quality measure which normally looks at correlation features between the pixels of original and reconstructed image. Normally NK is in the range of 0 to 1, very near to or one is the best. This is also known as a sliding dot product or sliding inner-product. It is expressed as

$$NK = \frac{\sum_{j=1}^M \sum_{k=1}^N x_{j,k} \cdot x'_{j,k}}{\sum_{j=1}^M \sum_{k=1}^N x_{j,k}^2}$$

Where x is the original image and x' is the denoised image, Where M , N are number of rows and columns of an image.

6.2.4 Normalized Absolute Error (NAE)

Normalized Absolute Error is the difference between the measured or inferred value of a quantity and its actual value. The large the value of NAE means that image is poor quality. It is given by

$$NAE = \frac{\sum_{j=1}^M \sum_{k=1}^N |x_{j,k} - x'_{j,k}|}{\sum_{j=1}^M \sum_{k=1}^N |x_{j,k}|}$$

Where x is the original image and x' is the denoised image, M and N is number of rows and columns of an image.

6.2.5 Structural Content (SC)

Structural count is actual difference between original and denoised image. It is co relational based quality measure which normally looks at correlation features between the pixels of original and reconstructed image. Normally SC is in

the range of 0 to1, very near to or one is the best. SC is defined as

$$SC = \frac{\sum_{j=1}^M \sum_{k=1}^N x_{j,k}^2}{\sum_{j=1}^M \sum_{k=1}^N x'_{j,k}^2}$$

Where x is the original image and x' is the denoised image, Where M and N is number of rows and columns of an image.

Quality measurements of table 3 images are compared with the original image to find dissimilarity between images. Quality measured values of those images are mentioned in the below tables.

Table 3: Quality measurements of various MRI brain images.

IQM/ Images	Image 1	Image 2	Image 3	Image 4	Image 5
MSE	44.0533	109.4396	70.6554	77.9763	59.0214
PSNR	87.7774	73.4776	68.2471	67.2612	70.0463
NCC	1.0347	1.0040	1.0070	1.0259	1.0242
AD	-1.0686	0.1630	-0.1806	-1.4602	-0.8766
SC	0.9181	0.9689	0.9712	0.9372	0.9419
MD	58	108	124	78	113
NAE	0.0213	0.0872	0.0929	0.1138	0.0868

From this table 3, the statistical measures of the PSNR values are higher than the MSE values. NCC & SC values are very close to 1, NAE values are low and MD, AD values are very favors so the novel approach gives the best result. Graphical based diagrammatic representation of above table is given in figure 5.

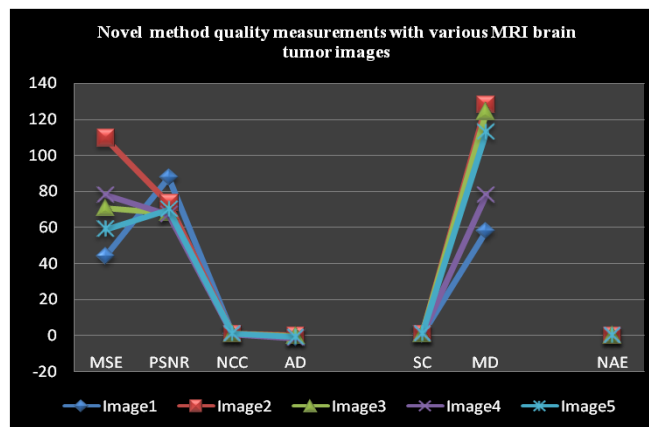


Figure 5: Novel method quality measurements with various brain tumor MRI images.

Different types of wavelet transforms are applied with the novel approach. This comparison made on many images, but here only two images (Image1, Image2) quality measurements are shown in table 4 and 5. Along with these wavelet transforms which technique contains the highest values of all these quality measurements except MSE is considered as a best result. Because that works well with the novel approach compared with other. From the result it is observes the haar wavelet transform gives better result than other wavelet transforms. So haar wavelet transform is used to decompose the image in SWT filter.

Table 4: Image1 Quality measurements of novel approach denoised image with various wavelet transforms.

IQM/ wavelets	Haar	DB	Smy	Coif	Bior	RBio
MSE	44.0533	59.8257	78.8209	79.2611	60.6547	70.8508
PSNR	87.7774	69.9109	67.1535	67.0978	69.7733	68.2195
NCC	1.0347	1.0401	1.0463	1.0465	1.0374	1.0367
AD	-1.0686	-1.9586	-1.1484	-1.1485	-1.0213	-1.0548
SC	0.9181	0.9123	0.8980	0.8976	0.9167	0.9154
MD	58	87	67	68	77	85
NAE	0.0213	0.0980	0.0916	0.0930	0.0841	0.0925

Figure 6 is the graphical representation of various types of wavelet transforms results with the given quality metrics in table4.

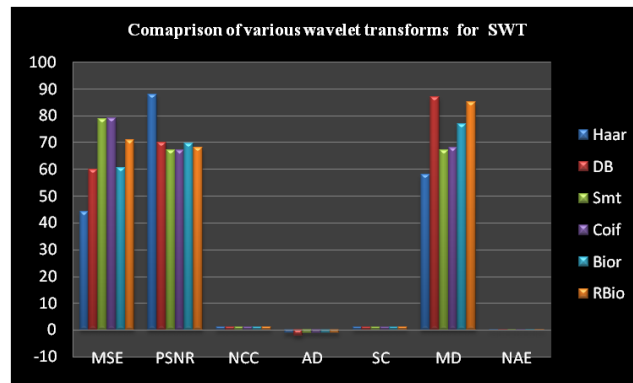


Figure 6: Comparison of various wavelets transforms.

Table 5: Image2 Quality measurements of novel approach denoised image with various transforms.

IQM/ Wavelets	Haar	DB	Sym	Coif	Bior	RBio
MSE	109.4396	271.1021	270.1382	266.3461	278.5668	300.0552
PSNR	73.4776	54.8003	54.8359	54.9773	54.5287	53.7856
NCC	1.0040	1.0081	1.0081	1.0082	1.0060	1.0054
AD	0.1630	-0.7024	-0.7170	-0.7076	0.2326	0.1042
SC	0.9689	0.9640	0.9640	0.9642	0.9673	0.9670
MD	108	223	205	197	218	245
NAE	0.0872	0.0813	0.0808	0.0804	0.0795	0.0871

Figure 7 is graphical representation for various wavelet techniques of SWT are compared and statistical report is given in table 5.

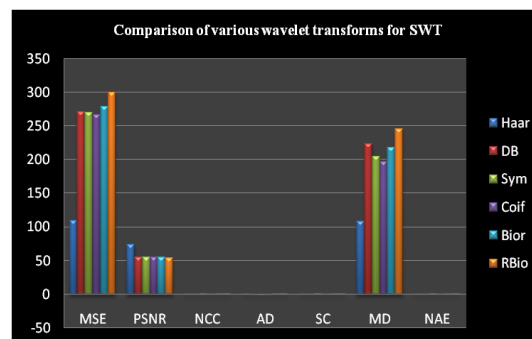


Figure 7: Comparison of various wavelets transforms.

The results of denoised image with three filtering techniques such as Median, Median with SWT filter and novel method filters are compared with the quality measures of various quality metrics. Among these wavelet transforms which technique contains the highest values of all these quality measurements except MSE is considered as a best result. From this result, it is observed that the denoised images of the novel method are providing better results.

Table 6: Quality measurements of denoised images based on median and SWT filters.

IQM/Filters	Median filter	Median & SWT filters	Novel method
MSE	88.9391	77.5264	44.0533
PSNR	73.9209	64.7788	87.7774
NCC	0.9899	0.9958	1.0347
AD	-1.1501	-1.8162	-1.0686
SC	1.0182	1.0049	0.9181
MD	98	83	58
NAE	0.0894	0.0516	0.0213

The statistical values of the quality measurements are among various filtering techniques are done of image1 and image2 are shown in table 6 and 7. And the graphical based diagrammatic representation of these two tables is given in figure 8 and 9. From these tables, it is observed that the quality measurements experimentally made between original and denoised image.

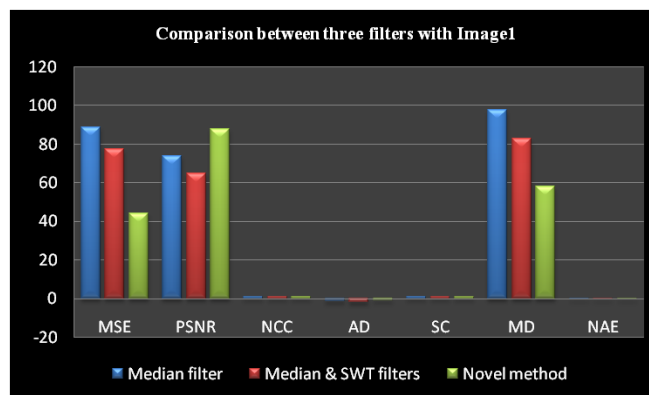


Figure 8: Comparison between three filters with image1.

Table 7: Quality measurements of denoised images based on median and SWT filters.

IQM/Filters	Median	Median & SWT	Novel method
MSE	399.7375	306.6644	109.4396
PSNR	67.8552	57.5143	73.4776
NCC	1.9811	1.9845	1.0040
AD	1.3117	0.3166	0.1630
SC	1.0227	1.0150	0.9689
MD	248	187	108
NAE	0.0949	0.0859	0.0872

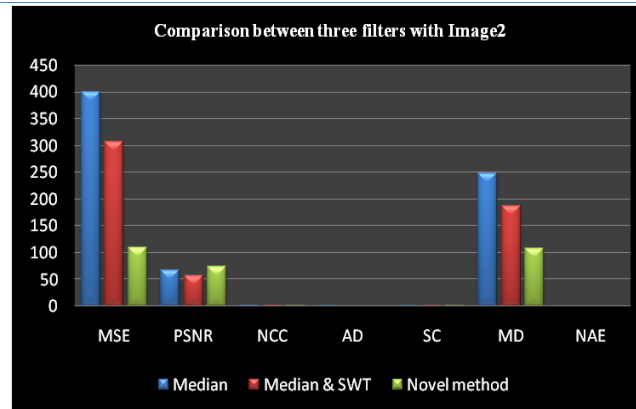


Figure 9: Comparison between three filters with Image2.

7 Conclusion

The results obtained using novel approach is applied in the various brain tumor MRI images and different types of wavelet transforms. This novel approach also compared with the various filtering techniques. It is clearly estimated and proved from the statistical measurements of this work that the novel approach is providing better results. So the denoising performance can be improved by choosing the better denoising techniques. The novel approach is produced the image with high perceptual quality and preservation of edge informations. From the overall work, it was verified that the single algorithm will never work better for all fields. In future, this approach is used for diverse applications.

REFERENCES

- [1] Abdullah Al Jumah, "Denoising of an Image Using Discrete Stationary Wavelet Transform and Various Thresholding Techniques", Journal of Signal and Information Processing,4, 33-41,2013.
- [2] D.Anithadevi, K.Perumal "Brain Tumour Extraction Based On Segmentation", International Journal on Recent and Innovation Trends in Computing and Communication (IJRITCC), ISSN: 2321-8169, Volume: 2 Issue: 9, 2682 – 2689,2014.
- [3] S. Janani, R.Marisuganya, R.Nivedha, "MRI Image Segmentation Using Stationary Wavelet Transform and FCM algorithm", International Journal of Computer Applications (0975 – 8887), ICIIOSP-2013.
- [4] Jaspreet kaur, Rajneet kaur," Image Denoising for Speckle Noise reduction in Ultrasound Images using dwt technique", International Journal of Application or Innovation in Engineering & Management (IJAEM), ISSN 2319 – 4847, Volume 2, Issue 6, June 2013.
- [5] Kanwaljeet Kaur, Gurjant Singh and Abhinash Singla, "Research On Spatial Filters And Homomorphic Filtering methods", Journal of Global Research in Computer Science (JGRCS), ISSN : 2229-371X, Volume 3, No. 11, November 2012.

- [6] Mirajkar PradnyaP., Sachine D. Ruikar, "Image Fusion based on Stationary Wavelet Transform", International journal of Advanced Engineering Research and Studies, II/ IV/July-Sept., 2013/99-101.
- [7] V N Prudhvi Raj, Dr. T Venkateswarlu, "Denoising of Medical Images using Image Fusion Techniques", International Journal of Signal and Image Processing, Vol.3 - Issue 4, April – 2012.
- [8] Ms. Rohini R. Varade, Prof. M. R. Dhotre, Ms. Archana B. Paturkar," A Survey on Various Median Filtering Techniques for Removal of Impulse Noise from Digital Images", International Journal of Advanced Research in Computer Engineering & Technology (IJARCET), ISSN: 2278 – 1323, Volume 2, Issue 2, February 2013.
- [9] Rong Zhu, Yong Wang," Application of Improved Median Filter on Image Processing", Journal of Somputers, vol. 7, no. 4, April 2012.
- [10] Rupinderpal Kaur, Ranjeet Kaur, "Remove the noise from Medical Images Using Discrete Wavelet Transform", International Journal of Engineering and Advanced Technology (IJEAT), ISSN: 2248 – 9622, Vol-3, Issue-2, April 2013,pp. 1611-1614.
- [11] C.Sasi varnan, A. Jagan, Jaspreet Kaur, Divya Jyoti, Dr.D.S.Rao, "Image Quality Assessment Techniques pn Spatial Domain", International Journal of Computer science and Technology,(IJCST), ISSN:2229-4333,Vol. 2 - Issue 3 ,2011.
- [12] Smrity Prasad, N.Ganesan," An Image Sharpening Method by Suppressing the Noise", International Journal of Computer Applications (0975 – 8887), Volume 51– No.16, August 2012.
- [13] Soundarya K, "Video Denoising based on Stationary Wavelet Transform and Center Weighted Median Filter", International Journal of Information Technology Bharati Vidyapeeth's Institute of Computer Applications and Management (BVICAM), Vol. 6 No. 1; ISSN 0973 – 5658, June-2014.
- [14] A.Velayudham, Dr.R.Kanthavel, "A Survey on Medical Image Denoising Techniques", International journal of Advanced research in Electronics and Communication Engineering (IJARECE), ISSN: 2278-909X, Volume 2, Issue 3, March 2013.
- [15] K.Vidyasagar, A.Bhujangarao, T.Madhu , " Noise Curtailment and Internsification of Brain Tumor MRI Images and its Area Estimation Using Segmentation and Clustering ", International Journal of Advanced Computing, ISSN: 2051-0845 , Volume 47, Issue 1, 2014.

An Accurate Liver Segmentation Method Using Parallel Computing Algorithm

Yousif Mohamed Y. Abdallah

*Department of Radiological Sciences and medical Imaging, College of Medical Applied Sciences,
Majmaah University
y.yousif@mu.edu.sa*

ABSTRACT

In liver, separating touching objects in an image is one of the more difficult image processing operations. Because of the presence of speckle noise in these images affects edges and fine details which limit the contrast resolution and make diagnostic more difficult. Thus, with using segmentation based algorithm, choice of appropriate segmentation technique type for each circumstance becomes an essential task. The watershed transform is often applied to this problem. The watershed transform finds "catchment basins" and "watershed ridge lines" in an image by treating it as a surface where light pixels are high and dark pixels are low. Segmentation using the watershed transform works well if one can identify, or "mark," foreground objects and background locations. This algorithm was done on twenty-five patients. A watershed transform Algorithm liver segmentation method was proposed in this study. Proposed method is able to determine the liver boundaries accurately. It is able to segment liver and improves radiological analysis and diagnosis.

Keywords: Text classification; Semantic Web with weighted idf feature; Expanded query; Fuzzy Semantic Web; Fuzzy Ranking Algorithm.

1 Introduction

A rapid sequence of images is acquired without table movement immediately after a bolus intravenous injection of radiographic contrast medium. The rate of enhancement in each pixel within the chosen slice can then be used to determine perfusion. The technique provides a quantifiable display of regional perfusion combined with the high spatial resolution afforded by CT. Computed tomography (CT) involves continuous patient translation during x-ray source rotation and data acquisition. As a result, a volume data set is obtained in a relatively short period of time. For chest or abdominal scanning, an entire examination can be completed in a single breath hold of the patient or in several successive short breath holds[1]. The data volume may be viewed as conventional transaxial images or with multiplanar and three-dimensional methods. The authors review the technologic aspects of spiral CT, as well as its advantages, limitations, and current clinical applications. Computed tomography (CT or CAT scan) is a noninvasive diagnostic imaging procedure that uses a combination of X-rays and computer technology to produce horizontal, or axial, images (often called slices) of the body[2]. A CT scan shows detailed images of any part of the body, including the bones, muscles, fat, and organs. CT scans are more detailed than standard X-rays. CT scans may be done with or without "contrast." Contrast refers to a substance taken by mouth

DOI: 10.14738/jbemi.23.1187

Publication Date: 31st May 2015

URL: <http://dx.doi.org/10.14738/jbemi.23.1187>

and/or injected into an intravenous (IV) line that causes the particular organ or tissue under study to be seen more clearly[3][4]. Contrast examinations may require fast manipulation for a certain period of time before the procedure. CT scans of the liver and biliary tract may also be used to visualize placement of needles during biopsies of the liver or during aspiration (withdrawal) of fluid from the area of the liver and/or biliary tract[5]. CT scans of the liver are useful in the diagnosis of specific types of jaundice (yellowing of CT scans of the liver and biliary tract (the liver, gallbladder, and bile ducts) can provide more detailed information about the liver, gallbladder, and related structures than standard X-rays of the abdomen, thus providing more information related to injuries and/or diseases of the liver and biliary tract [6][7]. CT scan of the liver and biliary tract may be performed to assess the liver and/or gallbladder and their related structures for tumors and other lesions, injuries, bleeding, infections, abscesses, unexplained abdominal pain, obstructions, or other conditions, particularly when another type of examination, such as X-rays, physical examination, and ultra sound is not conclusive [8]. A CT scan of the liver may be used to distinguish between obstructive and non-obstructive jaundice. Another use of CT scans of the liver and biliary tract is to provide guidance for biopsies and/or aspiration of tissue from the liver or gallbladder [9].

Image segmentation has been a long-standing problem in computer vision. It is a very difficult problem for general images, which may contain effects such as highlights, shadows, transparency, and object occlusion [10]. Segmentation in the domain of medical imaging has some characteristics that make the segmentation task easier and difficult at the same time. On the one hand, the imaging is narrowly focused on an anatomic region [11]. The imaging context is also well-defined. While context may be present to some extent in segmenting general images (e.g., indoor vs. outdoor, city vs. nature, people vs. animals), it is much more precise in a medical imaging task, where the imaging modality, imaging conditions, and the organ identity is known. In addition, the pose variations are limited, and there is usually prior knowledge of the number of tissues and the Region of Interest (ROI). On the other hand, the images produced in this field are one of the most challenging due to the poor quality of imaging making the anatomical region segmentation from the background very difficult [12][13]. Often the intensity variations alone are not sufficient to distinguish the foreground from the background, and additional cues are required to isolate ROIs. Finally, segmentation is often a means to an end in medical imaging [14]. It could be part of a detection process such as tissue detection, or for the purpose of quantification of measures important for diagnosis, such as for example, lesion burden which is the number of pixels/voxels within the lesion regions in the brain[15].

2 The Existing Ranking Methods

Separating touching objects in an image is one of the more difficult image processing operations. The watershed transform is often applied to this problem. The watershed transform finds "catchment basins" and "watershed ridge lines" in an image by treating it as a surface where light pixels are high and dark pixels are low. Segmentation using the watershed transform works well if one can identify, or "mark," foreground objects and background locations. Marker-controlled watershed segmentation follows this basic procedure:

1. Computation a segmentation function. This is an image whose dark regions are the objects I was trying to segment.
2. Computation the foreground markers. These are connected blobs of pixels within each of the objects.

3. Computation the background markers. These are pixels that are not part of any object.
4. Modification of the segmentation function so that it only has minima at the foreground and background marker locations.
5. Compute the watershed transform of the modified segmentation function.

Steps of liver segmentation using MatLab program showed in flowchart below:

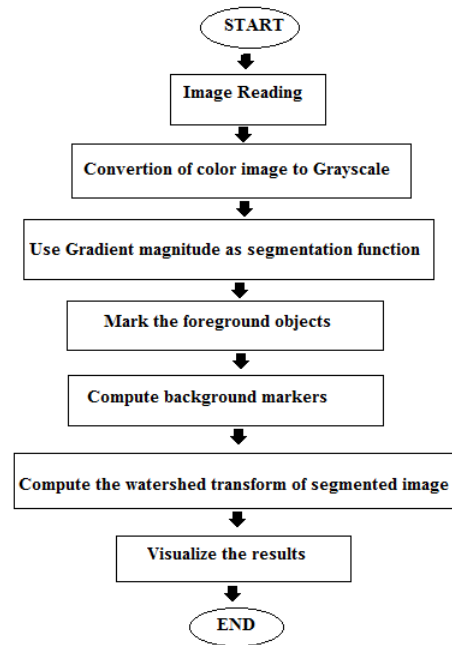


Figure 1. Steps of liver segmentation using MatLab program

3 The Results

Experimental study:

Step 1: Read in the Color Image and Convert it to Grayscale (Figure2)



Figure2 Original image used for liver segmentation

Step 2: Use the Gradient Magnitude as the Segmentation Function

The Sobel edge masks, imfilter, and some simple arithmetic were used to compute the gradient magnitude. The gradient is high at the borders of the objects and low (mostly) inside the objects (Figure3).

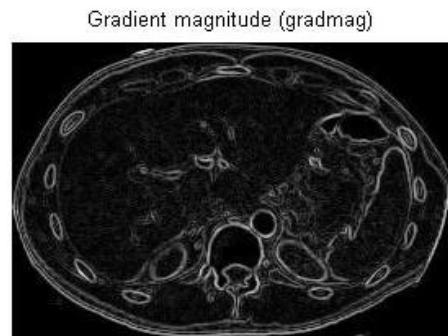


Figure 3. Gradient Magnitude as the Segmentation Function

The image was segmented by using the watershed transform directly on the gradient magnitude (Figure4).

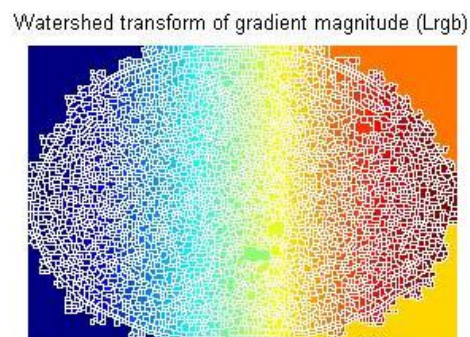


Figure 4. The watershed transform

Step 3: Mark the Foreground Objects

A variety of procedures could be applied here to find the foreground markers, which must be connected blobs of pixels inside each of the foreground objects. In this study morphological techniques were used and they called "opening-by-reconstruction" and "closing-by-reconstruction" to "clean" up the image. These operations will create flat maxima inside each object that can be located using `imregionalmax`.

Opening is an erosion followed by a dilation, while opening-by-reconstruction is an erosion followed by a morphological reconstruction (Figure5).

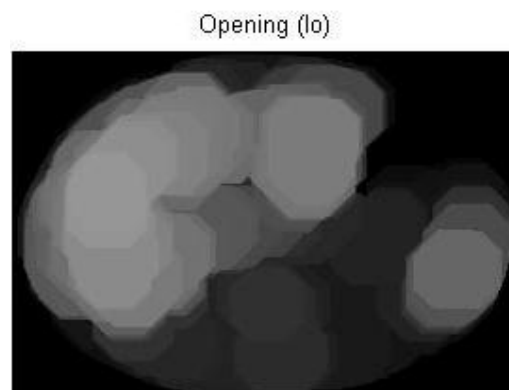


Figure 5. The Opening-by-reconstruction algorithm

Next the opening-by-reconstruction was computed using `imerode` and `imreconstruct` as shown in (Figure6).



Figure 6. The opening-by-reconstruction was computed using `imerode` and `imreconstruct`

Following the opening with a closing can remove the dark spots and stem marks. Compare a regular morphological closing with a closing-by-reconstruction. First `imclose` code was tried as shown in (Figure6).

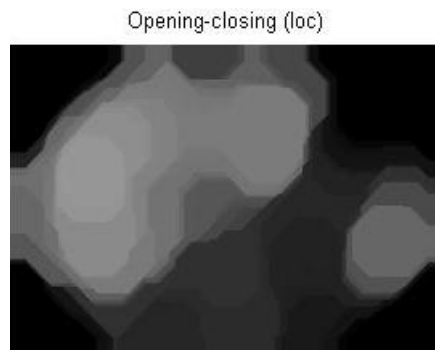


Figure 6. The 'Opening-closing algorithm

The `imdilate` code was used followed by `imreconstruct`. The image inputs and output of `imreconstruct` should complement as shown in (Figure7).



Figure 7. Opening-closing by reconstruction algorithm

When `lobrcbr` with `loc` were compared, reconstruction-based opening and closing found more effective than standard opening and closing at removing small blemishes without affecting the overall shapes of

the objects. Calculate the regional maxima of `lobrcbr` to obtain good foreground markers as shown in (Figure 8).

Regional maxima of opening-closing by reconstruction (fgm)

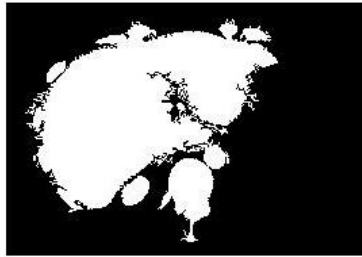


Figure 8. Regional maxima of opening-closing by reconstruction (fgm) filter

To help interpret the result, superimpose the foreground marker image on the original image as shown in (Figure9).

Regional maxima superimposed on original image (f2)

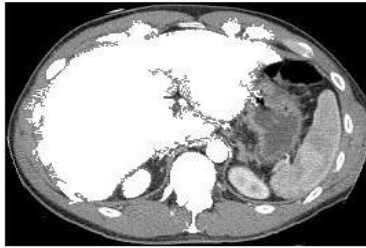


Figure 9. Regional maxima superimposed technique on original image

Some of the mostly-occluded and shadowed objects are not marked, which means that these objects will not be segmented properly in the end result. Also, the foreground markers in some objects go right up to the objects' edge. The edges of the marker blobs should clean and then shrink them a bit. This could be done by a closing followed by an erosion. This procedure tended to leave some stray isolated pixels that must be removed.

This could be done using `bwareaopen`, which removed all blobs that had less than a certain number of pixels as shown in (Figure10).

Modified regional maxima superimposed on original image (fgm4)



Figure 10. Modified regional maxima superimposed on original image

Step 4: Compute Background Markers

Now the background need to be marked. In the cleaned-up image, `lobrcbr`, the dark pixels belong to the background, a thresholding operation could start with as shown in (Figure11).

Thresholded opening-closing by reconstruction (bw)

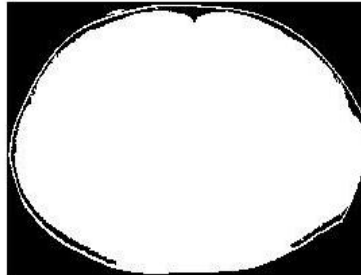


Figure 11. Thresholded opening-closing by reconstruction

The background pixels are in black, but ideally the background markers shouldn't to be too close to the edges of the objects which would segment. the background would "thin" by computing the "skeleton by influence zones", or SKIZ, of the foreground of `bw`. This can be done by computing the watershed transform of the distance transform of `bw`, and then looking for the watershed ridge lines ($DL == 0$) of the result.

Step 5: Compute the Watershed Transform of the Segmentation Function

The function `imimposemin` can be used to modify an image so that it has regional minima only in certain desired locations. Here `imimposemin` used to modify the gradient magnitude image so that its only regional minima occur at foreground and background marker pixels. Finally I compute the watershed-based segmentation using the following code:

```
L = watershed (gradmag2);
```

Step 6: Visualize the Result

One visualization technique is to superimpose the foreground markers, background markers, and segmented object boundaries on the original image. Dilation could use as needed to make certain aspects, such as the object boundaries, more visible. Object boundaries are located where $L == 0$ as shown in (Figure 12)

Markers and object boundaries superimposed on original image (I4)



Figure 12. Markers and object boundaries superimposed on original image

4 Conclusion

MatLab is an interactive system whose basic data element is an array that does not require dimensioning. This allows operators to solve many technical computing problems, especially those with matrix and vector formulations, in a fraction of the time it would take to write a program in a scalar non-interactive language such as C or FORTRAN. Magnetic resonance imaging (MRI) has become a common way to study liver. Information provided by medical images has become a vital part of today's patient care. The images generated in medical applications are complex and vary notably from application to application. The main objective of this research was to study an accurate liver segmentation method using a parallel computing algorithm. Computed Tomography images show characteristic information about the physiological properties of the structures-organs. In order to have high quality medical images for reliable diagnosis, the processing of image is necessary. The scope of image processing and analysis applied to medical applications is to improve the quality of the acquired image and extract quantitative information from medical image data in an efficient and accurate way. The main techniques of segmentation used in this study was watershed transform. The results of this technique agreed other author's' results who used different segmentation filtering based on the methods of enhance the computed tomography images. The watershed transform is often applied to solve the contrast and boundaries problem. The watershed transform finds "catchment basins" and "watershed ridge lines" in an image by treating it as a surface where light pixels are high and dark pixels are low. Segmentation using the watershed transform works well if one can identify, or "mark," foreground objects and background locations. This algorithm was done on twenty-five patients. A watershed transform Algorithm liver segmentation method was proposed in this study. Proposed method is able to determine the liver boundaries accurately. It is able to segment liver and improves radiological analysis and diagnosis.

REFERENCES

- [1] Abdallah, Y., Hayder, A., and Wagiallah ,E., Automatic Enhancement of Mammogram using Contrast Algorithm. *International Journal of Science and Research (IJSR)*, 2014. 3(9): p. 1886-1891.
- [2] Abdelwahab, R., and Abdallah, Y., Hayder, A., and Wagiallah ,E., Application of Texture Analysis Algorithm for Data Extraction in Dental X-Ray Images. *International Journal of Science and Research (IJSR)*, 2014. 3(10): p. 1934-1939.
- [3] Abdallah, Y., Alkhir, M., Algaddal, A., Improvement of Brain Tumors Detection Using Markers and Boundaries Transform. *International Journal of Science and Research (IJSR)*, 2015. 4(1): p. 2372-2378.
- [4] Bidgood, D. & Horii, S., Introduction to the ACR-NEMA DICOM standard. *RadioGraphics*, 1992. 12: p. 345-355.
- [5] Lehmann, T.M.; Gönner, C. & Spitzer, K., Survey: Interpolation Methods in Medical Image Processing. *IEEE Transactions on Medical Imagin*: 1999. 18(11): p. 1049-1075

- [6] Li, G. & Miller, R.W., Volumetric Image Registration of Multi-modality Images of CT, MRI and PET, Biomedical Imaging. Youxin Mao (Ed.), 2010.
- [7] Abdallah, Y., Application of Analysis Approach in Noise Estimation, Using Image Processing Program. Lambert Publishing Press GmbH & Co. KG, Germany, 2011.
- [8] Lyra, M.; Sotiropoulos, M., Lagopati, N. & Gavrilleli, M. , Quantification of Myocardial Perfusion in 3D SPECT images – Stress/Rest volume differences, Imaging Systems and Techniques (IST), IEEE International Conference 2010: p. 31 – 35
- [9] Narasimha-Iyer, H., et al., Automatic Identification of Retinal Arteries and Veins From Dual-Wavelength Images Using Structural and Functional Features. Biomedical Engineering, IEEE Transactions, 2007. 54(8): p. 1427-1435.
- [10] Abdallah, Y., and Wagiallah, E., Segmentation of Thyroid Scintigraphy Using Edge Detection and Morphology Filters. International Journal of Science and Research (IJSR), 2014. 3(11): p. 2768-2772.
- [11] Abdallah, Y., and Hassan, A., Segmentation of Brain in MRI Images Using Watershed-based Technique. International Journal of Science and Research (IJSR), 2015. 4(1): p. 683-688.
- [12] Hong, S., et al., Optimal scheduling of tracing computations for real-time vascular landmark extraction from retinal fundus images. Information Technology in Biomedicine, IEEE Transactions on, 2001. 5(1): p. 77-91.
- [13] Pinz, A., et al., Mapping the human retina. Medical Imaging, IEEE Transactions on, 1998. 17(4): p. 606-619.
- [14] Abdallah, Y., and Yousef R., Augmentation of X-Rays Images using Pixel Intensity Values Adjustments. International Journal of Science and Research (IJSR), 2015. 4(2): p. 2425-2430.

A Comparative Study of Shear-Wave Elastography and Strain Elastography on a Breast Phantom for Diagnosis of Tumor and Cyst

Mahdi Al-Qahtani¹, Eraj Humayun Mirza², Mubarak Dhafer Al-Qahtani³ and
Mohammed Fahad Al-Muqati⁴

*Department of Biomedical Technology, College of Applied Medical Sciences, King Saud University,
Riyadh, KSA*

¹amahdi@ksu.edu.sa, ²emirza@ksu.edu.sa, ³m.z_20@hotmail.com, ⁴king123-@hotmail.com

ABSTRACT

A lump in breast may suggest a possible development of breast cancer. As the tumor develops, it changes the physical property of the tissue by changing its stiffness. To detect the tumor generally mammography is performed. The findings of mammography are often inaccurate as it does not take into account the stiffness of tissue. Elastography is an imaging technique to measure the stiffness of tissues. In the current study, we have used a breast phantom to analyze differences between a tumor and a cyst via comparing shear-wave elastography and strain elastography techniques. Both the techniques performed equally for the diagnosis of tumour. However, it is suggested that strain elastography must be used in the diagnosis of a cyst as it provides enhanced details of the surrounding tissues.

Key-words: Elastography, Shear-wave, Strain, Ultrasound, breast, tumor, phantom.

1 Introduction

Changes in elasticity of tissue is attributed to pathological condition [1]. Various cancers appear as hard nodules as a result of increased density, while other diseases involves deposition of fat or collagen that might alter the tissue elasticity. Cysts filled with fluid may also be invisible to traditional ultrasound examination. In several cases, a diminished pathological lesion or a lesion that is not superficial may not be detected via conventional ultrasound technique [2]. Conventional ultrasound is a qualitative method [3], however there was a need to a more quantitative approach to differentiate healthy tissues from the diseased. To overcome this issue ultrasound elastography was introduced.

Elastography is a medical imaging technique that is non-invasive, which detects tumors according to their stiffness when compared to normal tissue.

Elastography is a non-invasive medical imaging technique. The purpose of this technique is detecting tumors based on their stiffness (elasticity) compared to normal tissue. Ultrasonic imaging used for the most common type of elastography to compare the shapes of the tissue under examination before and after it is compressed slightly. Normal tissue tend to be less stiff cancerous tumors. Elastogram is an image show as different shades of light and dark, also has different degree of stiffness. The elastogram show up

DOI: 10.14738/jbemi.23.1228

Publication Date: 17th June 2015

URL: <http://dx.doi.org/10.14738/jbemi.23.1228>

many tumors, including breast tumors better than conventional ultrasonic images. Elastography is an imaging modality that apply a small axial uniform compression on the tissue that provides insight into the elastic properties of biological tissue [4]. Currently two basic types of elastography is performed; the shear wave elastography (SWE) and strain elastography (SE) [5]. SWE uses a set of shear waves to measure the modulus of tissue and provides tissue stiffness based on pressure values determined by the machine [6, 7]. On the other hand SE make use of application of localized strain manually by the operator and determining the relative strain of a lesion in comparison to surrounding tissues [8, 9]. Recent studies have demonstrated similar use of both SWE and SE techniques individually for various tissues. However, their comparable results are not studied significantly. Here we report the evaluation of breast tumor in a phantom using both the SWE and SE techniques.

2 Materials & Methods

2.1 Elastography examination

SWE and SE was performed on elastography breast phantom. Breast tumor and cyst was identified using linear transducer with a bandwidth ranging from 4 – 15 MHz for SWE while 5 -15 MHz linear transducer was used for SE. After determining the tumor and cyst via B-mode ultrasound the SWE and SE elastography images were acquired and most crisp image was selected from a pool of several images. No compression was applied when performing SWE imaging, however in case of SE imaging a light compression was applied which was confirmed by the feedback loop in the machine itself.

This study was performed in accordance with guidelines followed by ethical review board of King Saud University (KSU). SE procedures were performed with SonixTouch Q+ from Ultrasonix Medical Corporation, 130-4311 Viking Way, Richmond, Canada, at Department of biomedical technology, College of applied Medical Sciences, KSU. SWE procedures were performed with Aixplorer from SuperSonic Imagine Les Jardins de la Duranne, Aix-en-Provence, France, at department of radiology, King Fahad Medical City. Elastography breast phantom was purchased from CAE healthcare USA, 6300 Edgelake Drive Sarasota, FL, USA.

2.2 Image evaluation

After the selection of appropriate image from the pool of several images from SWE and SE examination, the lesion size and area of tumor and cyst were recorded. Tissue stiffness for SWE was recorded as displayed in the machine. Results for SWE displayed blue coloration in the range of 30 kPa while the red color demonstrated tissue stiffness to be around 180 kPa. In case of SE, the strain ratio between normal and pathological tissue was measured. Blue coloration showing a soft tissue while red coloration demonstrating a hard tissue.

3 Results & Discussion

The images obtained from breast phantom using two different elastography machines were analyzed using Tsukuba elasticity score patterns [10]. It was observed that both the elastography equipment displayed similar images (figure 1B, 1D & 2B, 2D) in B-mode which was effective in differentiating a tumor from cyst. Furthermore it was observed that elastography patterns varied from equipment to equipment. A significant variation was observed among the color patterns of the tumor (figure 1A & 2A). The strain ratios were only measureable in SonixTouch Q+ ultrasound machine. The strain ratio was 0.17 for the

tumor observed. Furthermore, color patterns of cyst were also different. Aixplorer from Supersonic, depends on shear wave technology so it displays the cyst as cavity while all its surrounding tissue as normal tissue (figure 2A) whereas, on the other hand, the SonixTouch Q+ from Analogic depends on external compression, so it provides elastography images based on relative stiffness. It displays cyst in blue color as soft tissue while surrounding tissue as hard (red) in figure 2C

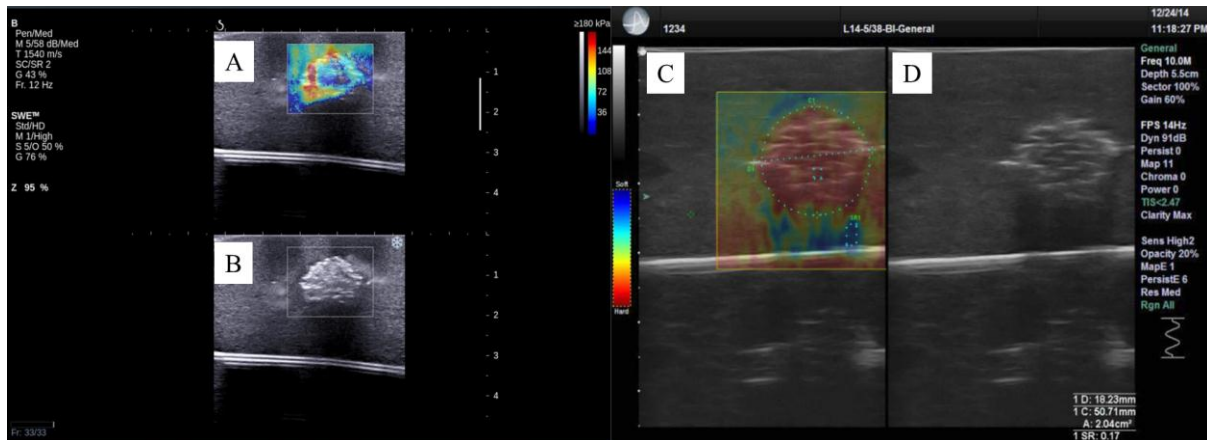


Figure 1: Figure A shows a tumor observed under SWE, B-mode ultrasound is shown in figure B and D. Figure C shows a tumor detected via SE.

In figure 1A SWE image for the tumor demonstrates that the left periphery of the tumor is stiffer than the right periphery. This tumor is expected to be soft in the middle while on the periphery as a whole the tumor is stiff. However contradicting results are visible in figure 1C where SE image shows a uniform high stiffness in the tumor. Although the periphery is less stiff than the tumor itself but a spread of tumor is suspected in the surrounding tissue.

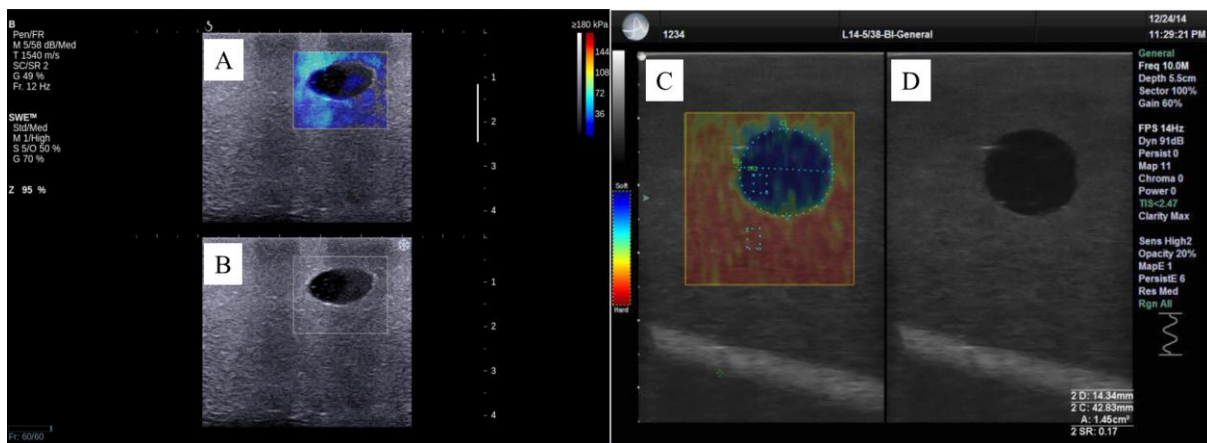


Figure 2: Figure A shows a cyst observed under SWE, B-mode ultrasound is shown in figure B and D. Figure C shows a cyst detected via SE.

Figure 2A displays a cavity with elastographic analysis. The blue area indicates that there is no stiff tissue while the uncolored black area is the cavity. However in figure 2C a cavity is shown in blue color while the surrounding tissue displays a stiff tissue in comparison to the cavity itself.

In our study, SWE and SE showed similar results. Both elastographic modalities improved diagnostic performance in combination with normal B-mode ultrasound. However, sensitivity was improved in SWE. These results are similar to that of Chang et al. [11], where they compared SWE and SE on benign and malignant breast lesions. Our results for cyst is the first of its kind. The cyst shows a normal tissue without any significant stiffness for SWE imaging, however a difference in tissue stiffness can be observed for surrounding tissue under SE imaging. We suggest imaging of cyst is definitely better under SE imaging as it might provide detailed strain ratios in case where there is inflammation of surrounding tissue. Whereas, in case of SWE, if there is a difference in tissue stiffness for surrounding tissue it might not be detected as SWE imaging shows the cyst as a cavity while its surrounding tissue is displayed as normal.

4 Conclusion

Both elastography techniques (SWE & SE) demonstrates promising future for diagnosis of breast tumours. However it is suggested that SE must be used for reviewing the cyst as it will provide more detailed diagnostic information for the surrounding tissue. Furthermore, Elastography must be combined with B-mode ultrasound to enhance the diagnostic performance.

ACKNOWLEDGEMENT

The authors extend their appreciation to the College of Applied Medical Sciences Research Center and the Deanship of Scientific Research at King Saud University for funding this research.

REFERENCES

- [1] Krouskop, T.A., et al., Elastic moduli of breast and prostate tissues under compression. *Ultrasonic imaging*, 1998. 20(4): p. 260-274.
- [2] Ophir, J., et al., Elastography: a quantitative method for imaging the elasticity of biological tissues. *Ultrasonic imaging*, 1991. 13(2): p. 111-134.
- [3] Manning, F.A., L.M. Hill, and L.D. Platt, Qualitative amniotic fluid volume determination by ultrasound: antepartum detection of intrauterine growth retardation. *American journal of obstetrics and gynecology*, 1981. 139(3): p. 254-258.
- [4] Ophir, J., et al., Elastography: ultrasonic estimation and imaging of the elastic properties of tissues. *Proc Inst Mech Eng H*, 1999. 213(3): p. 203-33.
- [5] Bamber, J., et al., EFSUMB guidelines and recommendations on the clinical use of ultrasound elastography part 1: Basic principles and technology. *Ultraschall in der Medizin*, 2013. 34(2): p. 169-184.
- [6] Cortes, D.H., et al., Continuous Shear Wave Elastography: A New Method to Measure Viscoelastic Properties of Tendons in Vivo. *Ultrasound Med Biol*, 2015.

- [7] Athanasiou, A., et al., Feasibility of Imaging and Treatment Monitoring of Breast Lesions with Three-Dimensional Shear Wave Elastography. *Ultraschall Med*, 2015.
- [8] Vural, M., et al., The evaluation of the retrobulbar orbital fat tissue and optic nerve with strain ratio elastography. *Med Ultrason*, 2015. 17(1): p. 45-8.
- [9] Park, H.J., et al., Strain elastography features of epidermoid tumors in superficial soft tissue: Differences from other benign soft tissue tumors and malignant tumors. *Br J Radiol*, 2015: p. 20140797.
- [10] Itoh, A., et al., Breast Disease: Clinical Application of US Elastography for Diagnosis 1. *Radiology*, 2006. 239(2): p. 341-350.
- [11] Chang, J.M., et al., Comparison of shear-wave and strain ultrasound elastography in the differentiation of benign and malignant breast lesions. *AJR Am J Roentgenol*, 2013. 201(2): p. W347-56.

Designing of Computer Aided Diagnostic System for the Identification of Exudates in Retinal Fundus Images

¹Santosh Kumar Mishra, ²Deepti Mittal and ³Ramesh Kumar Sunkaria

^{1,2}Electrical and Instrumentation Engineering Department, Thapar University, Patiala (Punjab), India;

³Department of electronic and communication, Dr.B.R. Ambedkar NIT Jalandher, jalandher, India

¹Santosh.mishra80135@gmail.com; ²deepti.mittal@thapar.edu; ³sunkariark@gmail.com

ABSTRACT

Macular edema is an advance stage of diabetic retinopathy which affects central vision of diabetes patients. The main cause of edema is the appearance of exudates near or on macular region in human retina. If the exudates are present in the macular region of retina, it will lead to diabetic macular edema. Early detection of macular edema in diabetic patients paves a path for prevention from blindness. The automatic system for early detection of diabetic macular edema should identify all possible exudates present on the surface of retina. In the proposed work, a computer added diagnosis system is design for the identification of the exudates in color retinal fundus images. The system consists of three stages; candidate exudates detection, feature extraction and classification. The system is designed with (i) background estimation, morphological reconstruction, normalization for candidate exudates detection (ii) Gray level co-occurrence matrix for feature extraction and (iii) support vector machine for classification. The classifier classifies in between the region of exudates and non-exudates. The system performance is evaluated in terms of the parameters such as sensitivity, specificity, mathews correlation coefficient, positive predicative value, and accuracy whose values are 88.23%, 100%, 88.23%, 100%, 93.75% respectively.

Keywords: Macular edema, Diabetic retinopathy, Exudate, Retina fundus images, Morphological reconstruction, Normalization, Candidate exudates detection,

1 Introduction

Diabetic retinopathy (DR) is a progressive eye disease that currently affects millions of people worldwide. Diabetic macular edema (DME) is a complication of diabetic retinopathy and it is a common cause of vision impairment and blindness [1]. DME is one of the complications caused by diabetes; DME may lead to visual damages in people at a working age. However, the risk of vision loss and blindness may be reduced if DME is detected early, and followed by appropriate treatment. DME occurs from swelling of the retina in diabetic patients due to leaking of fluid from micro aneurysms within the macula. This presentence of fluid causes retina thickening in diabetic patients which is termed lipid deposits also known as exudates. Exudates appear as bright structures with well-defined edges and variable shapes.

Study in medical imaging has shown that most of the exudates screen themselves in the human retina. This leads to a clear road for researchers to device and improve the method for analyzing exudates.

DOI: 10.14738/jbemi.23.1278

Publication Date: 05th July 2015

URL: <http://dx.doi.org/10.14738/jbemi.23.1278>

Therefore, specialized image processing method is used to obtain proper identification of exudates in retinal fundus images [2-3]. These image processing methods may help to medical professionals in timely diagnosis of DME and improve medical facilitation available to the patients.

There are two types of macular edema, (i) Non Clinically Significant Macular Edema (Non-CSME) and (ii) Clinically Significant Macular Edema (CSME). Non-CSME is a mild form of edema in which there are no symptoms of the disease because the locations of exudates are at a distance from fovea and the central vision is not affected. CSME is the severe form of edema in which the exudates leak out and get deposited very close to or on fovea affecting central vision of the eye [4]. Fig.1. is an example of retinal fundus image showing digital image of human retina along with its main components and exudates.

Many methods for diagnosing macular edema and other retinal diseases are discussed in literature [5-7]. Also exudates segmentation and classification method presented in the literature are based on: Thresholding and morphological methods, thresholding method analysis [8], Thresholding methods identify the exudates by local and global analysis of threshold whereas morphological methods first identify all the structure of predictable shape and removed them afterwards for easy detection of exudates in retinal fundus images [9-12]. Also, there are number of classification method to classify various lesion types in retinal images such as drusen, cottonwood spot, exudates [13-14]. In this work classification is performed in between exudates and non-exudates region on pixel to pixel basis, which will further aid to ophthalmologist in diagnosis of patient diabetic macular edema.

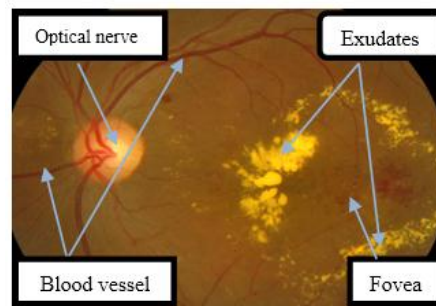


Figure 1.Digital fundus image of human retinal along with its main components and exudates

2 Background

The previous research works to identify exudates on retinal fundus images are based on two main criteria i.e., lesion based and image based, for assessing the diagnostic accuracy of exudates detection technique. In lesion-based criterion each abnormal retinal image can be segmented into a number of exudates regions. By considering a set of retinal image and applying an appropriate segmentation technique. The lesion based accuracy can be measured in terms of lesion sensitivity and specificity. The lesion-based accuracy can be assessed either in pixel-level basis or alternatively using large collection of pixel e.g., 10x10 slice. Exudates detection and identification was investigated by Phillips et al. [15,16]. The contrast of the exudates are enhanced, then after global and local thresholding values were used to segment exudates lesions. The sensitivity of this technique was reported between 61% and 100%, based on 14 images.

Ege et al. [17] locates exudates and cotton wool acne in 38 color images. These abnormalities were initially detected using a combination of templates matching, region growing, and thresholding technique.

Bayesian classifier based technique was classified the bright region into cotton wool spots, exudates and noise. The classification performance was only 62% for exudates and 52% for cotton wool spots.

Wang et al. [18] using the minimum-distance discriminate classifier to identify the retinal bright lesion such cotton wool and exudates. Neural network (NN) have been also classify the retinal exudates Another NN based exudates detection work was conducted by Hunter et al. The NN was trained to discriminate exudates from drusen based on 16x16 pixel slice. This technique achieved 100% sensitivity and 70% specificity.

Walter et al. [12] identified exudates from green channel of retinal image. After initial localization, the exudates are determined by mathematical morphology technique. This method had three parameter: size of local window, and two other threshold value. The first threshold find the minimum variation within each local window. The candidate exudates region based on first thresholding value. The second threshold changes the surrounding background pixels to be classify the exudates. This technique was achieved 92.8% sensitivity and 92.8%. predictivity asset of 15 abnormal retinal images.

Niemeijer et al. [19] distinguished the bright lesion, i.e., exudates, cotton wool spot, and drusen from color retinal images. In the first step, the image pixels are classified, in a lesion probability map that grouped into probable lesion pixel cluster characteristics, each probable cluster was assigned the likelihood that the cluster was a true bright lesion. these clusters were classified as exudate, cotton, wool spot, or drusen.

Goldbaum et al. [20] have discriminated similarly colored objects in retinal images based on color information, not many work have shown interest in color classification of retinal images.

Alireza et al. [21] proposed a method to automatic segment of exudates based on computational intelligent techniques. The color retinal image are segmented using fuzzy c-means clustering following some preprocessing steps, set of initial feature such as color, size, edge strength, and texture are extracted to classify these segmented image initial exudates and non-exudates region.

Ahmed et al. [22] proposed a method to automatically segment optic nerve and exudates. In the algorithms, they used preprocessing steps such as averaging filter, contrast adjustment, Thresholding, morphological opening, watershed transformation on the green component of the image. This method yielded sensitivity 96.7%.

Chugh et al. [23] detection of exudates such as uses homogeneity of healthy areas rather than unhealthy areas. In this method first extracted the healthy area such as optical nerve using sobel filter method and blood vessel by entropy thresholding method. Thresholding method is segmented exudates from diabetic retinopathy images. The proposed method yields accuracy 90%.

3 Material and method

3.1 Materials

MESSIDOR, a publicly available dataset is used to test performance of segmentation and classification for exudation. The MESSIDOR[24] dataset containing 80 fundus images with exudates region with Zeiss Visucam PRO fundus camera, at resolution of 1449x2201 pixel and with a 45° Field of view. The image

capturing process is vetted by automatic quality assessment algorithms based on the Elliptical local vasculature density feature [25-26].

3.2 Method

A method for the identification of exudates in fundus retinal images is presented which will further help in building a computer aided diagnostic system for macular edema. exudate, also known as bright lesions, appears as bright spots and patches in fundus image with highest contrast in the green channel of the color image. An automatic system for detection of exudates should enhance the contrast of bright region with smoothing the dark regions [27]. In this work, morphological reconstruction is used to smooth dark region such as haemorrhages and blood vessels [28]. The objective of contrast enhancement is to improve the contrast of lesion for easy detection. The image normalization technique used for detection all possible bright regions [29]. They are appropriate for texture representation and discrimination. The binary candidate region for exudates was extracted by applying a low adaptive Thresholding value [30]. The region was segmented by the thresholding, enhanced image also contain optical nerve region and pixel due to their similarity with exudates. For correct detection the false and unauthentic pixel should be removed before the classification stage. The proposed system segmented optical nerve using masking of related area where optical nerve probability in fundus image data base system.

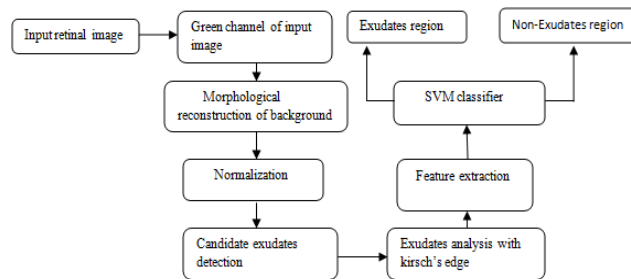


Figure.2. Proposed computer added diagnosis system for the identification of exudates in retinal fundus image

i) Selection: The green channel is selected because of better contrast of this channel than the rest two channels and it will further help in extracting the brightest region from the background.

ii) Preprocessing: Selected green channel of retinal fundus images are passed through various preprocessing steps in order to detect the region of exudates. The first step is the application of a big size median filter shown in the work of Niemeijer et al [31], which showed that the size of the median filter should be 1/30th of the height of the fundus image for background estimation. After that, the estimated background is subtracted from the original image. This step has a great computational performance advantage by avoiding multiple passes.

iii) Image normalization: Image normalization is the process where the highest intensity of the image is centered at zero. We enhanced the normalization with the addition of morphological reconstruction [29]. It improved the nerve fiber layer and other structures of edges of the optical nerve, without any expansion of the exudates region. The histogram showed a clear division between dark structures and bright structures. Dark structures like the macula and vasculature are located on the left side of the histogram. On the other hand, bright structures are formed on the positive side of the histogram, which contain the optical nerve and bright lesions.

such as exudates and other structure related to very bright retinal pigment epithelium layer. Because of the alignment of the histogram after the normalization we can select all exudates candidate region.

The method of optical nerve removal [32], it is understandable that the similarity of potential of color between optical nerve and exudates in fundus image. The optical nerve detection is the mature technique. So we only concentrate to exudate detection. We did not implement automatic optical nerve detection in our paper. We did manual removal of optical nerve by the having size slightly greater than optical nerve.

iv) Exudate edge detection: The exudate detection is performing by conveying a score for each exudates candidate. The exudate candidates are selected by running 8-neighbour connected component analysis of exudates candidate region. The way of implementation is based on Kirsch's Edges [33]. The advantage of this method to take the higher inner and outer edge value of exudates in compare to non-exudates structure. Kirsch's edges try to capture the external edges of the lesion candidate. This edge detection is based on kernel K to evaluate at 8 different directions. The kernel output are combined together by selecting the maximum value found on each pixel output

It computes the gradient by convolution the image with eight template impulse response arrays as shown in figure. The scalar factor is 1/15.

$$K = \begin{matrix} \frac{5}{15} & \frac{-3}{15} & \frac{-3}{15} \\ \frac{5}{15} & \mathbf{0} & \frac{-3}{15} \\ \frac{5}{15} & \frac{-3}{15} & \frac{-3}{15} \end{matrix} \quad (1)$$

The gradient of different direction is obtained by convolving the image with eight impulse response arrays. The final gradient is set to be a large gradient among different direction. Thus edge is enhanced by Kirsch's method. The threshold is set after edge enhancement to determine if a pixel belongs to the edge or not.

Thresholding based technique focus on a global or adaptive gray level analysis, but the automatic selection of proper Thresholding is difficult due to uneven illumination of the image.

v) Feature Extraction: Feature extraction involves simplifying the amount of resources required to describe a large set of data accurately. The large number of variable generally requires a large number of memory and computational power or a classification algorithm. Texture plays a significant role in image analysis and pattern recognition. In this proposed method, Gray level co-occurrence matrix (GLCM) is formulated to obtain statistical texture features. There are two types of texture feature measures. They are first order and second order measures. GLCM is the second order texture calculation. In second order texture measures consider relationship between neighbors. But first order texture measures are statics, consider not pixel neighbor relation. Texture features have high discrimination accuracy, requires less computation time and hence efficiently used for real time Pattern recognition applications.

GLCM is defined over an image to be distribution of co-occurrence values at a given offset; GLCM is a matrix where the number of row and columns is equal to the number of gray level. The use of statistical feature is one of the early proposed methods in the image processing literature. Haralic [34] suggested the use of co-occurrence matrix of GLCM. The feature extraction from GLCM is Energy, Contrast, Entropy, Correlation and Homogeneity.

1. **Contrast-** it is a measurement of intensity contrast between a pixel and its neighborhood pixels in the whole image.

$$\text{Contrast} = \sum_{i,j} |i - j|^2 p(i, j) \quad (2)$$

2. **Correlation** – It is a measure of how a pixel is correlated to its neighborhood pixel in whole image.

$$\text{Correlation} = \sum_{i,j} \frac{((i - \mu_i)(j - \mu_j) p(i - j))}{\sigma_i \sigma_j} \quad (3)$$

3. **Energy** – It is the sum of squared elements in GLCM. It ranges from 0 to 1. For constant image, energy value is 1.

$$\text{Energy} = \sum_{i,j} p(i, j)^2 \quad (4)$$

4. **Homogeneity** – The closeness measurement of the elements distribution in GLCM to GLCM diagonal.

$$\text{Homogeneity} = \sum_{i,j} \frac{p(i, j)}{1 + |i, j|} \quad (5)$$

vi) Classification: Classification based technique supervised approaches attempt to extract different feature and then use a classifier to classify the exudates and non-exudates region. Support vector machine (SVM) classifier is used to classify the Exudates and Non-Exudates regions. SVM is a supervised learning model with associated learning algorithms that analyze data and recognize patterns, used for classification and regression analysis. The basic SVM takes a set of input data and predicts, for each given input. The classification process is divided into training phase and testing phase. The known data is the training phase and unknown data is the given in testing phase. The accuracy depends on the efficiency of the classification.

vii) Measurement and performance evaluation: Different measures are used to evaluate the performance of the system. The measures used are Accuracy, Mathews correlation coefficient (MCC), Sensitivity, Specificity and Positive prediction value (PPV). These values are calculated from the Confusion Matrix [35]. A confusion matrix contains information about actual and predicted classifications done by a classification system. Performance of such systems is commonly evaluated using the data in the matrix.

TN (True negative) - correct prediction as normal

FN (False negative) - incorrect prediction of normal

FP (False positive) - incorrect prediction of abnormal

TP (True positive) -correct prediction of abnormal

The accuracy is the percentage of prediction that is correct

$$\text{Accuracy} = (TP + TN) \div (TP + FP + TN + FN) \quad (6)$$

The Matthews correlation coefficient is used in machine learning as a measure of the quality of binary classifications.

$$MCC = (TP \times TN - FP \times FN) \div (\sqrt{(TP + FP)(TP + FN)(TN + FP)(TN + FN)}) \quad (7)$$

The sensitivity is the percentage of positive level instances that were predicted as positive.

$$\text{Sensitivity} = (TP) \div (TP + FN) \quad (8)$$

The specificity is the percentage of negative labeled instance that were predicted as negative.

$$\text{Specificity} = (TN) \div (TN + FP) \quad (9)$$

The Positive Prediction Value or precision rate is the percentage of positive prediction is correct.

$$PPV = (TP) \div (TP + FP) \quad (10)$$

4 Result and discussion

4.1 Green channel separation:

The abnormalities are more visible in the green channel. So separation of green channel from RGB images is needed. The separate green channel images is show in figure 3(a).

4.2 Median Filter and Background estimation

4.2.1 Median filter:

In the green channel, noise is present. Hence median filter is using. The median filter is non linear digital filter technique. It's proved to be best in removing salt & pepper and Impulse noise. Median filter erased black dots called the pepper and fills in white holes in the image, called salt. It better works than mean filter by preserving sharp edges. It simply replaces each pixel value by the median of the intensity level in the neighborhood of the pixel. As can be seen figure 3(b). Here using the big size window of median filter because saving the bright region of the image.

4.2.2 Background estimation:

Due to using median filter some bright region information are lost. For recovering of that information we are estimating the background. As shown in figure 3(c). In retinal image database containing 1449x2201 pixel configurations, where 1449 rows are present there. So in result (49x49) size of median filter window, this result is good contrast between exudates and background. This approach has great computational performance advantage avoiding the multiple passes. After that estimated background is subtracted from the original image in order to obtain a normalized version, in proposed method, enhanced the normalization with morphological reconstruction.

4.3 Morphological reconstruction:

In morphological reconstruction process one image called the marker, based on the character of another image, called masked. The high point and the peak in the marker image specify where processing begins. The peaks spared out or dilate while being forced to fit within the mask image. The scattering processing continues until the image value stop changing as shown in figure 3(e).

4.4 Image normalization:

In image normalization technique, the dark and bright region is classified shown in figure 3(e). Histogram of normalized image shown that all pixels centered at zero shown in figure 3(f). The normalized image is called exudate candidate detection.

4.5 Edge detection and global thresholding:

After image normalization we want to detect the external edge of the exudates candidate region, Using Kirsch's edge detection. Kirsch's operator is non-linear edge detector that find maximum edge strength in few predetermine direction. The operator takes a single kernel mask and rotates it in 45° increment through all compass direction. The edge magnitude of the kirsch operator is calculated as the maximum magnitude across all direction, and the resultant image is shown in figure 2(f).

Global thresholding is used to convert an intensity image to binary image. Level is a normalized intensity value that lies in the range [0 1]. Then threshold to minimize the intra class variance of the black and white pixels. Final exudates segmented image is shown in figure 3(g).

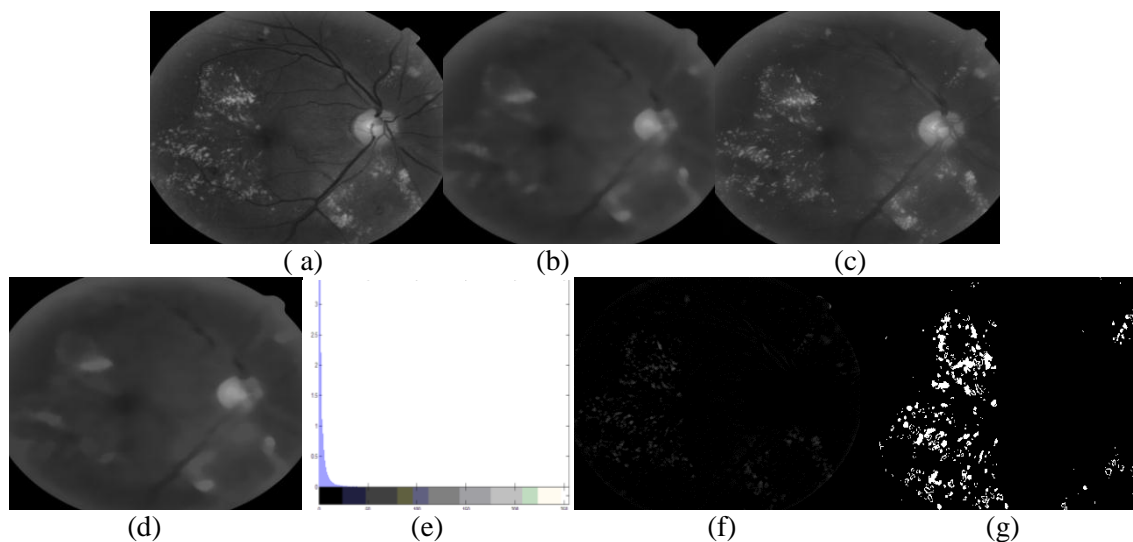


Figure.3. a, b, c, d, e, f, g: green channel image, median filtered image, background estimation image, morphological image, histogram of normalized image, exudates candidate detection, exudates segmented image.

4.6 Feature extraction:

The GLCM feature of exudates and non-exudates segmented region of the image is extracted. The size of the exudates and non-exudates region is equal. The segmented region of exudates and non-exudates regional size is (10x10) pixel.

The randomly select the slice of 42 exudates and 40 non-exudates region from 9 different retinal fundus images. And find the mean \pm variance of GLCM properties like contrast, correlation, energy and homogeneity of exudates and non-exudates regions.

Table1: GLCM feature values in terms of mean ± variance

Mean±Variance	Contrast	Correlation	Energy	Homogeneity
Exudates	0.1041±0.0032	0.7652±0.0245	0.4898±0.0187	0.9591±0.0008
Non-exudates	0.1825±0.0156	0.3329±0.0334	0.6031±0.0524	0.9087±0.0038

4.7 SVM classifier:

For the proposed work, 82 slices of images were chosen randomly feature is extracted and its classification was obtained. The construct feature sets are separately tested using the SVM classifier .The SVM structure depends on the training set and testing set from feature like area, contrast, correlation, and homogeneity are given as input to SVM. To train the network 82 retinal images were taken than the system is loaded with the statistical features, which are, contrast, correlation, energy, and homogeneity of retinal image from the workspace or from file. There are 17 images of testing for exudates region and corresponding 15 testing image for Non-exudates region .The computational result are presented

Table2: Confusion matrix for exudates classification

Parameter	Segmented exudates
TP	15
FP	0
FN	2
TN	15

The performance of proposed system is measured using sensitivity, specificity, PPV, accuracy and MCC. Sensitivity is true positive rate. Specificity is true negative rate. Table 3 clearly shows that the designed computer aided system to diagnose AMD out performs the other existing methods in terms of its performance by measuring Sensitivity, specificity, PPV, Accuracy, MCC.

Table 3: Comparative performance evolution of proposed computer aided diagnostic system with existing method

Method	Sensitivity	Specificity	PPV	Accuracy	MCC
Wang et al [18]	-	70	-	-	-
Walter et al [12]	92.74	100	92.39	-	-
Ahmed et al [22]	96.7	100	94.9	-	-
Osareh et al [21]	93	94.1	-	93.4	-
Akram et al [5]	-	-	-	-	94.73
Proposed method	88.23	100	100	93.75	88.23

5 Conclusions

The proposed work presents the designing of computer aided diagnostic system for identification of exudates in retinal fundus images. System consists of three phases these are candidate exudates detection, feature extraction, and classification. The bright region is enhanced and segmented using morphological reconstruction, image normalization and global thresholding. Normalization procedure gives a substantial computational advantage to our method. The median filter and morphological reconstruction gives good contrast of foreground image. Feature set of each candidate region is formed using different properties of exudate and non-exudate region. We implemented a SVM based classifier to

divide the region into exudate and non-exudate regions. The results demonstrated that the proposed system can be used in computer aided diagnosis system for DR as it identified and detected exudates with high accuracies.

REFERENCES

- [1] D. E. Singer, D. M. Nathan, H. A. Fogel, and A. P. Schachat, "Screening for diabetic retinopathy." *Ann Intern Med*, vol. 116, no. 8, 1992. P: 660–671.
- [2] M. D. Abramoff, M. Niemeijer, M. S. A. Suttorp-Schulten, M. A. Viergever, S. R. Russell, and B. van Ginneken, "Evaluation of a system for automatic detection of diabetic retinopathy from color fundus photographs in a large population of patients with diabetes." *Diabetes Care*, vol. 31, no. 2, 2008. P: 193–198.
- [3] S. Philip, A. D. Fleming, K. A. Goatman, S. Fonseca, P. McNamee, G. S. Scotland, G. J. Prescott, P. F. Sharp, and J. A. Olson, "The efficacy of automated "disease/no disease" grading for diabetic retinopathy in a systematic screening programme." *Br J Ophthalmol*, vol. 91, no. 11, 2007.P:1512–1517.
- [4] M.D. Abramoff, M.K. Garvin, Sonka, M., "Retinal Imaging and Image Analysis," *IEEE reviews in Biomedical Engineering*, vol.3, 2010. P:169.
- [5] M. U. Akram and S. A. Khan, "Automated detection of dark and bright lesions in retinal images for early detection of diabetic retinopathy", *Journal of Medical System*, vol.36, no.5, 2011.P:3151-3162.
- [6] A. Tariq, M. U. Akram, A. Shaukat, S. A. Khan, "Automated Detection and Grading of Diabetic Maculopathy in Digital Retinal Images", *Journal of Digital Imaging*, vol. 26, no. 4, 2013. P: 803-812, 2013.
- [7] M. U. Akram, A. Tariq, M. A. Anjum, M. Y. Javed, "Automated Detection of Exudates in Colored Retinal Images for Diagnosis of Diabetic Retinopathy", *OSA Journal of Applied Optics*, vol. 51 no. 20,2012.P: 4858-4866.
- [8] R. Phillips, J. Forrester, and P. Sharp, "Automated detection and quantification of retinal exudates, " *Graefes Arch Clin Exp Ophthalmol*, vol. 231, no. 2,1993. P: 90–94.
- [9] C. Sinthanayothin, J. F. Boyce, T. H. Williamson, H. L. Cook, E. Mensah, S. Lal, and D. Usher, "Automated detection of diabetic retinopathy on digital fundus images," *Diabetic Medicine*, vol. 19, no. 2,2002.P: 105–112.
- [10] H. Li and O. Chutatape, "Automated feature extraction in color retinal images by a model based approach," *IEEE Transactions on Biomedical Engineering*, vol. 51, no. 2, 2004. P: 246–254.

- [11] T. Walter, J. K. Klein, P. Massin, and A. Erginay, "A contribution of image processing to the diagnosis of diabetic retinopathy—detection of exudates in color fundus images of the human retina." *IEEE Transactions on Medical Imaging*, vol. 21, no. 10, 2002.P: 1236–1243.
- [12] A. Sopharak, B. Uyyanonvara, S. Barman, and T. H. Williamson, "Automatic detection of diabetic retinopathy exudates from non-dilated retinal images using mathematical morphology methods." *Computerized Medical Imaging and Graphics*, vol. 32, no. 8, 2008.P: 720–727.
- [13] D. Mittal, V. kumar, S. C. Saxena, N.Khandelwal, "Neural networks based focal liver diagnosis using ultrasound images," *Computerized Medical Imaging and Graphics*, vol.35,no-4,2011.P:135-323.
- [14] K. Kumari, D. Mittal, "Automated Drusen Detection Technique for Age-Related Macular Degeneration" *Society for science and education, united kingdom*,vol.2,2015,P:19-26.
- [15] R. Phillips, T. Spencer, P. Ross, P. Sharp, and J. Forrester, "Quantification of diabetic maculopathy by digital imaging of the fundus," *Eye*, vol. 5, 1991.P: 130–137.
- [16] R. Phillips, J. Forrester, and P. Sharp, "Automated detection and quantification of retinal exudates," *Graefe's Arch. Clin. Exp. Ophthalmol.*, vol. 231, 1993.P: 90–94, 1993.
- [17] B. Ege, O. Larsen, and O. Hejlesen, "Detection of abnormalities in retinal images using digital image analysis," in *Proc. 11th Scand. Conf. Image Process.*, vol. 13,2009.P: 833–840.
- [18] H. Wang, H. Hsu, K. Goh, and M. Lee, "An effective approach to detect lesions in retinal images," in *Proc. IEEE Conf. Comput. Vis. Pattern Recogn.*, Hilton Head Island, vol. 2, 2000. P: 181–187.
- [19] M. Niemeijer, B. V. Ginneken, S. R. Russell, M. Suttorp, and M. D. Abramoff, "Automated detection and differentiation of drusen, exudates and cotton-wool spots in digital color fundus photographs for diabetic retinopathy diagnosis," *Invest. Ophthalmol. Vis. Sci.*, vol. 48, 2007. P: 2260–2267.
- [20] M. Goldbaum, S. Moezzi, A. Taylor, and S. Chatterjee, "Automated diagnosis and image understanding with object extraction, object classification and inferencing in retinal images," in *Proc. IEEE Int. Conf. Image Process.*, Lausanne, Switzerland, vol. 3,1996.P: 695–698.
- [21] Alireza O., B. Shadgar and R. Markham, "A Computational-Intelligence- Based Approach for Detection of Exudates in Diabetic Retinopathy Images", *IEEE Trans on Information Tech in Biomedicine*, vol. 13, No.4, 2009. P: 535-545.
- [22] Ahmed Wasif Reza, C. Eswaran, Subhas Hati, "Automatic Tracing of Optic Disc and Exudates from Color Fundus Images Using Fixed and Variable Thresholds", *Journal of Medical Systems*, vol. 33,2009.P: 7380.

- [23] S. Chugh, J Kaur, and D. Mittal, "Exudates segmentation in retinal fundus image for detection of Diabetic retinopathy", *IJERT*, vol.3, 2014. P:673-677.
- [24] Methods to evaluate segmentation and indexing techniques in the field of retinal ophthalmology. [Online]. Available: <http://messidor.crihan.fr>
- [25] L. Giancardo, M. Abramoff, E. Chaum, T. Karnowski, F. Meriaudeau, and K. Tobin, "Elliptical local vessel density: a fast and robust quality metric for retinal images," in *Conf. of the IEEE EMBS*, 2008.
- [26] L. Giancardo, "Quality Assessment of Retinal Fundus Images using ELVD". *IN-TECH*, 2010, ch. *New Developments in Biomedical Engineering*, 2010. P: 201–224.
- [27] D. Mittal, V.Kumar, S.C.saxena, N. khandewal and N. kalra "Enhancement of the ultrasound images by modified anisotropic diffusion method". *Med. Biol. Engg. computer.*, vol.48, no-12, 2010. P:1281-1291
- [28] L. Vincent, "Morphological grayscale reconstruction in image analysis: applications and efficient algorithms," *IEEE Journal of Image Processing*, vol. 2, no. 2, 1993. P: 176–201.
- [29] A. D. Fleming, S. Philip, K. A. Goatman, J. A. Olson, and P. F. Sharp, "Automated microaneurysm detection using local contrast normalization and local vessel detection," *IEEE Transactions on Medical Imaging*, vol. 25, no. 9, 2006. P: 1223–1232..
- [30] C. I. Sanchez, M. Garca, A. Mayo, M. I. Lopez, and R. Hornero, "Retinal image analysis based on mixture models to detect hard exudates." *Medical Image Analysis*, vol. 13, no. 4, 2009. P: 650–658.
- [31] M. Niemeijer, B. van Ginneken, J. Staal, M. S. A. Suttorp-Schulten, and M. D. Abramoff, "Automatic detection of red lesions in digital color fundus photographs," *IEEE Trans Med Imag*, vol. 24, no. 5, 2005. P: 584– 592.
- [32] J. Kaur, D. Mittal "Segmentation and Measurement of Exudates in Fundus Images of the Retina for Detection of Retinal Disease." *Society for science and education, united kingdom*, vol.2. 2015. P:28-38.
- [33] R. A. Kirsch, "Computer determination of the constituent structure of biological images." *Computers and Biomedical Research*, vol. 4, no. 3, 1971. P: 315–328.
- [34] K. Shanmugam, R. M. Haralick and I. H. Dinstein, "Textural features for image classification" *IEEE Transactions on Systems, Man and Cybernetics* 3, 1973. P: 610 – 621.
- [35] R. Kohavi and F. Provost. *Glossary of terms, Special Issue on "Applications, of Machine Learning and the Knowledge Discovery Process"*, *Journal of Machine Learning*, vol. 30, 1998. P: 271–274.